Journal of Physical Science and Application 8 (2) (2018) 1-10
doi: 10.17265/2159-5348/2018.02.001

Influence of Pulsed Power Transmission on Radio Wave Environment

Hisayoshi Sugiyama

Department of Physical Electronics and Informatics, Osaka City University, Osaka 558-8585, Japan

Abstract: Influence of pulsed power transmission on radio wave environment is investigated. The power pulses are transmitted intermittently in pulsed power network that is already proposed for an alternative of upcoming smart grids. In contrast to conventional power transmission with continuous electric current of low frequency sine wave, pulsed power transmission may affect surrounding field with high frequency radio noises. In this paper, based on the analysis of electric field strength around a power line, the radio noises generated by various forms of pulsed power transmission are evaluated. As a result, two points are derived. First, though the total of generated radio noise power obviously exceeds that of conventional power transmissions, peak strength of electric field rather falls behind the conventional one. Second, concerning the influence on the radio wave of the lowest frequency 40 kHz that is actually used for standard time and frequency signal, the noise intensity possibly exceeds the weak radio signal tolerance according to the shape of each power pulse transmitted.

Key words: Smart grid, power packet, energy packet, radio noise.

1. Introduction

As one of the upcoming smart grids [1], pulsed power network is proposed to distribute electric power effectively over consumers in a power network [2, 3]. In this scheme, time axis is equally divided into frames and each frame is subdivided into a fixed number of power slots. These frames and power slots are synchronized over the network with GPS time signals [4]. Power transmission is decomposed into a series of electric pulses located at specified power slots in successive frames. These power slots are pre-reserved throughout the power transmission path without any confliction against other paths that already exist. The power path reservation is executed by the coordination of end nodes and intermediate power routers with decentralized algorithm [3]. The power routers directly relay the pulsed power transmission without additional relay loss.

The fundamental advantages of this scheme are as follows: First, it has affinity with dispersion type power sources such like photovoltaic power generations and wind turbine generations. In current power systems, reverse power flow to power lines from these power sources conflicts with existing power flow. This confliction may cause problems including the degradation of power line quality at neighboring consumers [5]. In contrast, such problems do not occur in the pulsed power network because no conflictions occur among power transmission paths that are pre-reserved individually.

Second, it has manageability of energy coloring in the process of power distribution. Energy coloring means the attachment of associated information to each power transmission [6, 7]. This additional information includes the charge of the pulsed power segment, the type of its energy source, and the source location. This information enables consumers to select the electric power of the lowest charge, or to select the attribute of energy source concerning greenhouse gas emissions or such global scale problems.

Third, high reliability and flexibility of power systems is obtained especially when the systems suffer from disasters. The reliability means that a partial

Corresponding author: Hisayoshi Sugiyama, Ph.D., associate professor, research field: telecommunications.

failure of the system does not affect extensive part of the system. This reliability is brought by the scheme of decentralized control by every node in the system. On the other hand, the flexibility means that critical facilities such like hospitals can be supplied power selectively in emergencies.

One of the problems that arise from this scheme of pulsed power network is the potential influence on radio wave environment around the power lines where the pulsed power transmission is executed. In contrast to the conventional power transmission with continuous electric current of low frequency sinusoidal wave, the spectrum of a chopped waveform of pulsed power transmission includes higher harmonics with noticeable intensity that possibly generates serious radio noises around the power lines.

In this paper, the influence of the pulsed power transmissions on surrounding radio wave environment is investigated. Because the weak radio signal tolerance is regulated in Japanese radio law where the radio noise is defined by the electric field intensity at a specified frequency, the influence of the pulsed power transmission is estimated as follows:

First, the electric field intensity generated by the pulse flow is calculated at frequencies around that of conventional sine wave power transmission. Then, the peak intensity over the frequencies is compared with that of conventional power transmission. Second, because the lowest frequency radio wave service "standard radio signal" is within LF (low frequency) band, the electric field intensity within the band is calculated and compared with the weak radio signal tolerance.

In Section 2, the electric field intensity around a power line with continuous sinusoidal current is formulated. In Section 3, several waveforms of pulse train in one frame are specified for the radio noise calculation. In Section 4, the electric field intensity generated by the pulse trains is calculated. The influence on radio wave environment is investigated around the frequency of conventional sinusoidal power transmission, and in LF band where actual services are operated. In the final section, the investigations are summarized and subjects are discussed for further studies.

2. Electric Field Intensity around a Power Line

The radio noise intensity is regulated in Japanese radio law as the electric field intensity at the evaluation point. The evaluation point is at 3 m distant from the noise source. According to this regulation, the electric field intensity E is analyzed around a straight wire where sinusoidal electric current flows.

Fig. 1 shows the analysis model of the intensity E [V/m] around the wire. In this xyz-coordinate system, the wire stretches along z-axis from $-z_m$ to z_m where electric current flows. The intensity of the current $I(t; z)$ is expressed as:

$$I(t, z) = A\exp\{j\omega(t - z/c)\} \quad (1)$$

where, A means the amplitude of the current, ω means the angular frequency, and c means the velocity of the current flow. The velocity c is assumed to equal light velocity.

The evaluation point of the electric field strength E is at (0, R, 0) in this coordinate system. E is decomposed into its y -component E_y and z-component E_z. E_x does not exist because of the field symmetry. These components of E and the maximum field strength E_{max} at the evaluation point are derived as[1]:

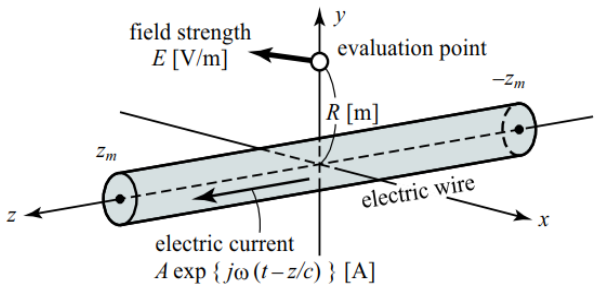

Fig. 1 Electric field intensity E at the evaluation point.

[1] The derivation processes of these formulas are shown in the Appendix.

$$E_y = \frac{-AR\omega\mu}{2\pi}\int_0^{z_m} \frac{z\sin(\omega z/c)\exp\left(-j(\omega/c)\sqrt{R^2+z^2}\right)}{(R^2+z^2)^{(3/2)}}dz \tag{2}$$

$$E_z = j\frac{-AR^2\omega\mu}{2\pi}\int_0^{z_m} \frac{\cos(\omega z/c)\exp\left(-j(\omega/c)\sqrt{R^2+z^2}\right)}{(R^2+z^2)^{(3/2)}}dz \tag{3}$$

$$E_{max} = \sqrt{\sqrt{a^2+b^2}+d} \tag{4}$$

where, μ and c are the permeability and light velocity, respectively. a, b, d in the last equation are expressed as:

$$\begin{cases} a = \left(E_{yr}^2 + E_{zr}^2 - E_{yi}^2 - E_{zi}^2\right)/2 \\ b = E_{yr}E_{yi} + E_{zr}E_{zi} \\ d = \left(E_{yr}^2 + E_{zr}^2 + E_{yi}^2 + E_{zi}^2\right)/2 \end{cases} \tag{5}$$

where, E_{yr} and E_{yi} mean the real and imaginary part of E_y, respectively. Similarly, E_{zr} and E_{zi} mean the components of E_z.

In the actual calculation of these values, z_m is set large enough so as to reach the integrations converge.

3. Pulse Trains in Each Frame

In pulsed power network, time axis is divided equally into frames synchronized over the network. Each synchronized frame continues T [sec] and is subdivided into N equivalent power slots of τ [sec] length ($\tau = T/N$) where electric pulses are transmitted at pre-reserved positions [3].

Three shapes of the electric pulse train in one synchronized frame are indicated by Fig. 2. The horizontal axis represents the time and the vertical axis represents the electric current.

There are two design concepts of the shape of each electric pulse. In Fig. 2, (a) and (b) are designed with the first concept whereas (c) is designed with the second one.

With the first concept, the shape should be designed to be similar to a part of sinusoidal wave that is used in conventional power transmissions. In Fig. 2, (a) and (b) are designed with this concept. Each electric pulse of these pulse trains is specified by the biased cosine wave:

$$I_{bc}(t) = (A_{bc}/2)\{1 - \cos(2\pi t/\tau)\}, \tag{6}$$

where, domain of t equals [0, τ], and A_{bc} means the amplitude of the pulse as shown in the figure. From now on, the electric pulse of this shape is referred to as BC pulse.

The purpose of this design concept is to suppress the higher harmonics in the spectrum of the electric pulses and to design the spectrum almost identical to that of conventional power transmission where only the fundamental wave exists. With this first concept, the influence of the pulsed power transmission on radio wave environment may become similar to that of the conventional power transmission, and additional influence caused by the higher harmonics may be suppressed.

In the pulse train (a), M BC pulses are concatenated in each frame. This concatenation makes the shape of pulse train close to the conventional sinusoidal wave and suppresses the higher harmonics in its spectrum. Especially when M equals N, both waveforms are equalized with each other except for the direct component and no higher harmonics arise whereas in (b), the positions of M BC pulses are randomized. Those random positions of pulses possibly appear in actual operations of pulsed power networks.

However, with this first concept, the pulse shape management becomes difficult throughout the power transmission path. Within the path, the nonlinear relay characteristics of power routers possibly distort the waveform of transmitted pulses.

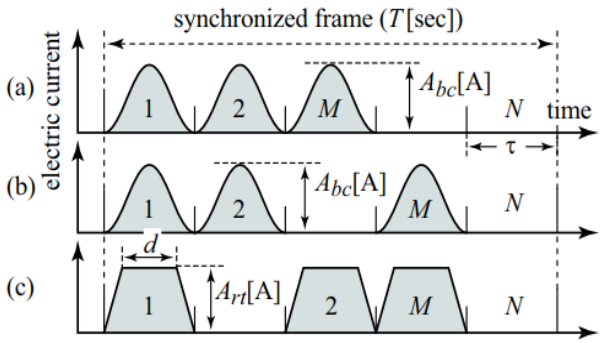

Fig. 2 Pulse trains adopted for noise spectrum evaluation.

In contrast, pulse train (c) in Fig. 2 is designed with the second concept. With this concept, the shape of electric pulses is designed to a simple rectangle. In the figure, considering the actual signal processing where some rise and fall times exist, upper base width d is assumed. From now on, this rectangle pulse is referred to as RT pulse. A_{rt} means the RT pulse amplitude.

Obviously, the sharp corners of the rectangle generate intensive high harmonics that cause noticeable influence on radio wave environment. However, though the total volume of the radio noise increases, this shape spreads the noise power over wide spectrum range. Therefore, possibly the peak intensity rather falls behind that of conventional power transmission by sinusoidal wave where the spectrum of noise power concentrates on the fundamental frequency.

Apparently, with this second concept, electric pulse relaying by power routers becomes feasible. The relaying is accomplished by simple switching and almost no disturbance occurs caused by the nonlinearity of routers.

4. Noise Spectrum Evaluation

As the radio wave noise is caused by pulsed power transmission, the spectrum of electric field strength E_{max} is derived adopting three cases of pulse trains indicated in Fig. 2. In each case, the pulse train is Fourier-transformed into the fundamental wave and its harmonics. The electric field strength E_{max} of each Fourier component is calculated by Eq. (4). In the calculation, frame length T and number of power slot N are set to 1 s and 100, respectively. Therefore, the power slot width τ equals 10 (m·s)[2]. The distance R of the evaluation point from the wire is set to 3 m according to the weak radio signal tolerance in Japanese radio low. Upper base width d of RT pulse is set to 6 m·sec.

[2] From this value, the frequency of electric pulse repetition bacomes 100[Hz]. This frequency is reasonable from the view point of reasonableness of existing power systems designed for 50 or 60[Hz] oscillation.

In the following subsections, first, E_{max} is calculated at frequencies around 60 Hz that is typical frequency of conventional sinusoidal power transmissions. Then, the influence of electric pulse train on radio wave environment is evaluated in comparison with that of the conventional power transmission.

Second, the electric field strength E_{max} within LF band is calculated. In LF band, the lowest frequency radio wave service “standard radio signal” is operated. Therefore, calculation of E_{max} in this band and the result evaluation in comparison with the weak radio signal tolerance is necessary.

In the calculations, pulse amplitudes A_{bc} and A_{rt} indicated in Fig. 2 are adjusted to make the value of root mean square I_{rms} of each pulse equivalent to that of pure sine wave. I_{rms} indicates the effective current of power transmission. For example, if I_{rms} is set to 1 A, the amplitude of the sine wave, BC pulse, and RT pulse become 1.414 A, 1.633 A, and 1.168 A, respectively.

4.1 Radio Noise around the Frequency of Conventional System

The noise spectrums derived are shown in Figs. 3-5. In these figures, effective current I_{rms} are set to 1 A. Horizontal axis represents the frequency [Hz] and vertical axis represents the electric field strength E_{max}[V/m].

Fig. 3 shows the noise spectrum of the pulse train (a) and sine wave of 60 Hz. As the pulse train, two cases of M (99 and 50) are evaluated. These noise spectrums are indicated by solid line and dashed line, respectively.

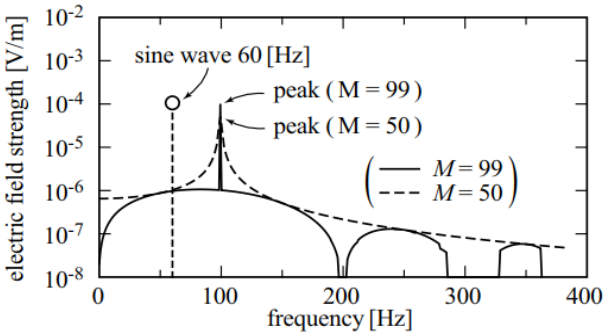

Fig. 3 Noise spectrum of pulse train (a) and pure sine wave.

The peak strength E_{max} of the former (M = 99) is 1.011×10^{-4} V/m at 100 Hz. Whereas, that of the latter (M= 50) is 0.510×10^{-4} V/m. Both peak values appear at 100 Hz that is the repetition frequency of electric pulses. On the other hand, radio noise E_{max} of the conventional sine wave is 1.061×10^{4} V/m at 60 Hz.

From Fig. 3, following two points are recognized.

(1) As described in Section 3, the noise spectrum of pulse train designed by the first concept becomes similar to that of sine wave especially when the large number of pulses is concatenated. The effect of this design concept is confirmed by the figure. For example, the noise spectrums around the pulse repetition frequency 100 Hz are different apparently between the cases of M equals 99 and 50.

(2) Though the total volume of radio wave noise apparently increases, the peak noise intensity of pulsed power transmission rather falls a little behind conventional sine wave power transmission. The reason is the effect of noise power dispersion over wide range of frequencies. Therefore, concerning this peak noise intensity compared with the conventional power systems, the influence of pulsed power transmission on radio wave environment is not so serious regardless of the volume of current flows.

Fig. 4 shows the noise spectrum of the pulse train (b) where M is set to 50. The peak strength E_{max} is 0.510×10^{-4} at 100 Hz. Because of the randomized positions of electric pulses, the noise spectrum somewhat fluttered. However, the peak strength equals that of pulse train (a) of the same M. This peak value depends only on the number of pulses M in a frame regardless of their positions.

Fig. 5 shows the noise spectrum of the pulse train (c) where M is set to 99. In this case, E_{max} appears as 6.746×10^{-5} V/m at 200 Hz. Because of the rectangle pulses with sharp corners, the effect of noise power dispersion increases in comparison with BC pulse trains. Therefore, the peak intensity E_{max} decreases noticeably even though the number of pulses M equals 99 and almost of power slots are occupied.

4.2 Radio Noise around the Frequency of Actual Operation

In this subsection, the influence of pulsed power transmission on radio wave environment of low frequency range around 40 kHz is investigated where standard time signal waves are broadcasted as the lowest radio wave service.

At this low frequency range, the maximum electric field strength E_{max} is derived by Eq. (4). Differing from the previous subsection, the effective current I_{rms} of each pulse and conventional sine wave is varied from 1 A to 1,000 A. This range is fixed concerning the maximum allowable current 470 A of overhead distribution line [8].

First, the noise spectrum of BC wave with 99 pulses is shown in Fig. 6. The horizontal axis represents the frequency around 40 kHz and this center frequency is indicated by dashed line. The vertical axis represents

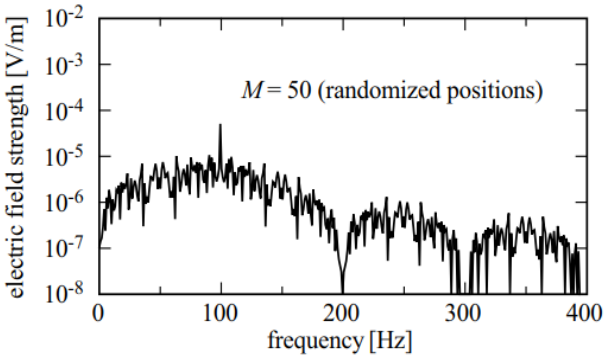

Fig. 4 Noise spectrum of pulse train (b).

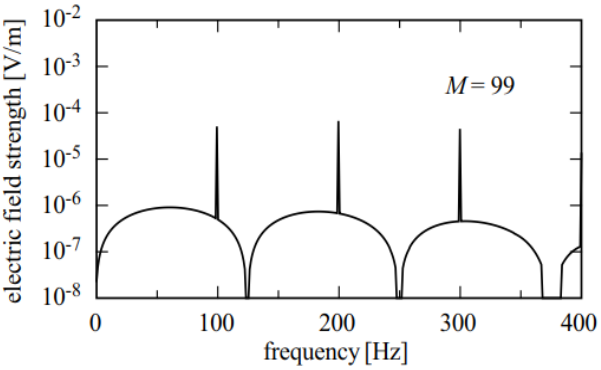

Fig. 5 Noise spectrum of pulse train (c).

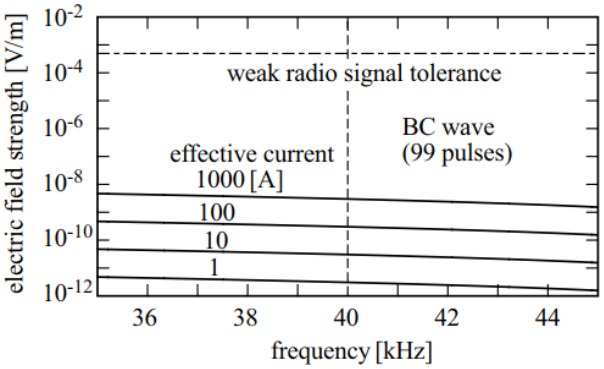

Fig. 6 Noise spectrum of pulse train (a) around 40 kHz.

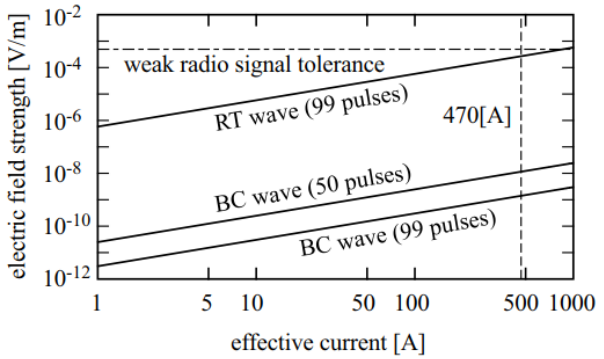

Fig. 7 Noise intensity of pulse trains at 40 kHz.

the electric field strength E_{max} V/m. Four values of effective current: from 1 to 1,000 A are adopted as the parameter. In comparison with the weak radio signal tolerance indicated by dot-dash line, the influence of radio noise by this case of pulse train on actual radio services at low frequency band may not be serious.

As Fig. 6 shows, the noise intensity gradually decreases in low frequency range. Therefore, concerning the radio noise influence on actual radio wave service, standard time signal waves, the influence at 40 kHz, the lowest frequency of the service is essential.

Fig. 7 shows the radio noise intensity at this critical frequency 40 kHz by three cases of the pulse train. Horizontal axis represents the effective current. The vertical axis represents the same as Fig. 6. The maximum available current 470 A of overhead distribution line is indicated by a dashed line.

This figure shows two points. First, the influence by RT wave becomes noticeable at 40 kHz in comparison with the weak radio signal tolerance. Second, because of the pulse shape designed to suppress the higher frequency components, BC wave has less influence on other radio wave services regardless of the number of pulses in each frame.

5. Conclusion

Influence of pulsed power transmission on radio wave environment is investigated. In contrast to conventional power transmission with continuous electric current of low frequency sine wave, pulsed power transmission may affect surrounding field with high frequency radio noises. In this paper, the radio noises generated by various forms of pulsed power transmission are evaluated. As the results, two points are derived. First, though the total of generated radio noise power obviously exceeds that of conventional power transmissions, peak strength of electric field that appears at the repetition frequency of electric pulses rather falls behind the conventional one. Second, concerning the influence on the radio wave of the lowest frequency 40 kHz that is actually used for standard time and frequency signal, the noise intensity possibly exceeds the weak radio signal tolerance regulated by Japanese radio law provided the rectangle pulses are transmitted.

As the results, biased cosine pulses and their concatenated form are confirmed to be suitable to avoid the influence of pulsed power transmission on radio wave environment, especially when existing radio wave services in LF band such as standard radio signal are concerned. Therefore, in further studies, the detailed operation scheme of electric pulse generation and transmission should be investigated. This subject includes the design of inverter circuit to generate biased cosine wave accurately and the design of power router that relays the biased cosine shaped current without any waveform distortion.

References

[1] Gungor, V. C., Sahin, D., Kocak, T., Ergut, S., Buccella, C., Cecati, C., et al. 2011. "Smart Grid Technologies: Communication Technologies and Standards." *IEEE*

Trans. Industrial Informatics 7 (4): 529-39.

[2] Sugiyama, H. 2013. "Direct Relayed Power Packet Network with Decentralized Control for Reliable and Low Loss Electrical Power Distribution." In *Proceedings of the GCCE2013*, pp. 32-36, Oct. 2013.

[3] Sugiyama, H. 2015. "Pulsed Power Network Based On Decentralized Intelligence For Reliable and Low Loss Electrical Power Distribution." *JAISCR* 5 (2): 97-108.

[4] Brandao, R. F. M., Carvalho, J. A. B., and Barbosa, F. M. 2006. "GPS Synchronized Measurements in Power Systems State Estimation: An Overview." *UPEC'06*, Sept. 2006.

[5] Hatta, H., Asari, M., and Kobayashi, H. 2009. "Study of Energy Management for Decreasing Reverse Power Flow from Photovoltaic Power Systems." In *Proceedings of the SAE2009*, pp. 1-5, Sept. 2009.

[6] Kato, T., et al. 2009. "Appliance Recognition from Electric Current Signals for Information-Energy Integrated Network in Home Environments." *Int. J. Assistive Robotics and Systems* 10 (4): 51-60.

[7] Saito, K., and Okabe, Y. 2011. "Quality-Aware Energy Routing Toward On- Demand Home Energy Networking." In *Proceedings of the CCNC2011*, Jan. 2011.

[8] Japan Electrotechnical Standards and Codes Committee. 2013. "JEAC 6001-20013".

[9] Slater, J. C., and Frank, N. H. 1969. *Electromagnetism.* Dover Publications.

Appendix

A. Electric field made by a current element

Consider a power line on z-axis with electric current $A\exp\{j\omega(t-z/v)\}$ as Fig. 8 shows, where, v means the velocity of the current flow that can be assumed almost to the light velocity. Based on this assumption, consider the electric field E that is made only by the electric current element of width d located on the origin of z-axis.

From now on, time component $\exp(j\omega t)$ in formulas is omitted. Then, the amplitude of the current is expressed by $A\exp(-j\omega z/v)$ and especially that of the current element equals A where z equals 0.

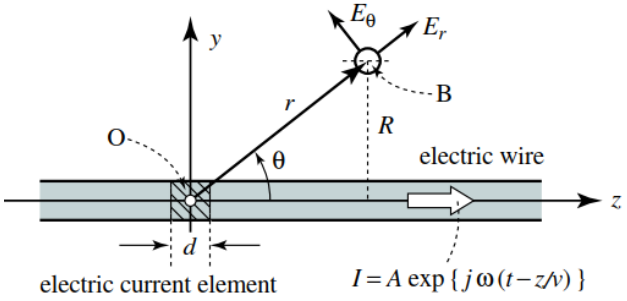

Fig. 8 Electric field E made by an electric current element at the origin of coordinate.

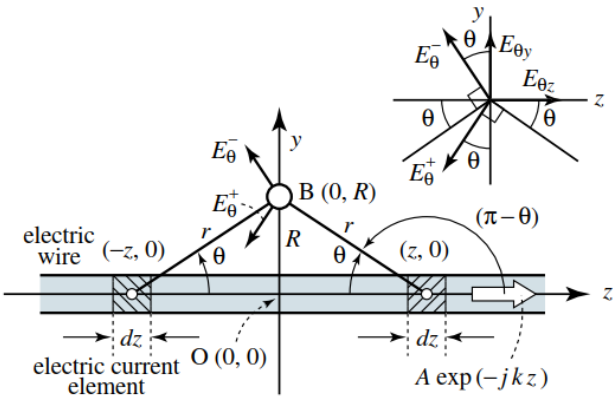

Fig. 9. Electric field E made by two current elements symmetrical with respect to the origin of z-axis.

Based on this analysis model, the electric field E at the evaluation point "B" is derived as [9]:

$$\begin{cases} E_\theta^{(1)} = j\dfrac{\eta Ad}{2\lambda r}\sin\theta\,\exp(-jkr) \\ E_r^{(3)} = \dfrac{Ad}{j\,2\pi r^3\omega\varepsilon}\cos\theta\,\exp(-jkr) \\ E_\theta^{(3)} = \dfrac{Ad}{j\,4\pi r^3\omega\varepsilon}\sin\theta\,\exp(-jkr), \end{cases} \tag{7}$$

where, r means the distance of "B" from the origin, θ means the angle of the direction to "B" from z-axis. E_r and E_θ are electric field components of E orthogonal to each other. The direction of E_r equals that of "B" from the origin.

Within the term that expresses E_θ, $E_\theta^{(1)}$ means the term that is proportional to $(1/r)$. Similarly, $E_r^{(3)}$ and $E_\theta^{(3)}$ mean the terms that are proportional to $(1/r^3)$.

k, η, and λ are wave number, wave impedance, and wave- length, respectively. They are expressed as:

$$k = \omega\sqrt{\varepsilon\mu},\quad \eta = \sqrt{\mu/\varepsilon},\quad \lambda = 2\pi/k \tag{8}$$

From now on, the electric field derived in this subsection made by the current element is referred to as elemental field.

B. Electric field made by a power line

The electric field E made by the power line indicated in Fig. 1 can be derived by the integration of the elemental field over z-axis. Here, these policies are set.

(1) Among the equations (7), only the first one that is inversed proportional to r is considered and others are omitted. Because the first equation indicates the radio wave generation caused by high frequency electric current and others indicate static field unrelated with the frequency.

(2) The velocity of the current flow in the power line is assumed to equal the light velocity (=$1/\sqrt{\varepsilon\mu}$). As the result, current $A\exp\{j\omega(t - z/v)\}$ becomes $A\exp(j\omega t - jkz)$. Furthermore, the current is expressed as $A\exp(-jkz)$ where $A\exp(j\omega t)$ is omitted.

With these policies, the electric field E is derived by the following procedure. These descriptions are graphically compensated by Fig. 9 (From now on, the coordinate is expressed by (z, y)).

(1) Derive the electric fields E_θ^+ and E_θ^-. These are the field at the evaluation point B on y-axis (0, R) made by the current elements at (z, 0) and ($-z$, 0), respectively.

(2) Compose the derived E_θ^+ and E_θ^-, and calculate z and y-direction component $E_{\theta z}$ and $E_{\theta y}$, respectively. The relation among E_θ^+, E_θ^-, $E_{\theta z}$ and $E_{\theta y}$ is shown in the upper-right part of Fig. 9.

(3) Apply Eq. (8), $r = \sqrt{R^2 + z^2}$, $\sin\theta = R/r$, and $\cos\theta = z/r$ to the derived $E_{\theta z}$ and $E_{\theta y}$, and arrange the formulas.

(4) Replace d with dz in $E_{\theta z}$ and $E_{\theta y}$ and integrate them with respect to z. The integral values are expressed by E_z, E_y, respectively. The integration range is set to $[0, z_{max}]$. z_{max} is set large enough so as to reach the integration converges.

(5) Derive the electric field E by composing the integral values E_z and E_y. First, calculate $E_z^A = \mathrm{R}[E_z\exp(j\omega t)]$ and $E_y^A = \mathcal{R}[E_z\exp(j\omega t)]$[3]. These values are the actual strength of the electric field of z-axis and y-axis component, respectively. Finally, derive the actual strength of the electric field E by composing the derived E_z^A and E_y^A.

According to this procedure, followings are derived.

Procedure 1:

$$\begin{cases} E_\theta^+ = j\dfrac{\eta d}{2\lambda r}A\exp(-jkz)\sin(\pi-\theta)\exp(-jkr) \\ \quad\ = j\dfrac{\eta Ad}{2\lambda r}\sin\theta\exp\{-jk(r+z)\} \\ E_\theta^- = j\dfrac{\eta d}{2\lambda r}A\exp(jkz)\sin\theta\exp(-jkr) \\ \quad\ = j\dfrac{\eta Ad}{2\lambda r}\sin\theta\exp\{-jk(r-z)\} \end{cases} \tag{9}$$

Procedure 2:

$$\begin{cases} E_{\theta y} = E_\theta^-\cos\theta - E_\theta^+\cos\theta \\ \quad\ = (E_\theta^- - E_\theta^+)\cos\theta \\ E_{\theta z} = -\left(E_\theta^-\sin\theta + E_\theta^+\sin\theta\right) \\ \quad\ = -(E_\theta^- + E_\theta^+)\sin\theta \end{cases} \tag{10}$$

In the equations above, $(E_\theta^- - E_\theta^+)$, and $(E_\theta^- + E_\theta^+)$ are expressed as:

$$\begin{cases} E_\theta^- - E_\theta^+ = j\dfrac{\eta Ad}{2\lambda r}\sin\theta\cdot\alpha \\ E_\theta^- + E_\theta^+ = j\dfrac{\eta Ad}{2\lambda r}\sin\theta\cdot\beta, \end{cases} \tag{11}$$

respectively. α, β are expressed as follows:

[3] $\mathcal{R}[\ ]$ means the real part of the complex number.

$$\begin{cases} \alpha = \exp\{-jk(r-z)\} - \exp\{-jk(r+z)\} \\ \quad = \exp(-jkr)\cdot 2j\sin(kz) \\ \beta = \exp\{-jk(r-z)\} + \exp\{-jk(r+z)\} \\ \quad = \exp(-jkr)\cdot 2\cos(kz) \end{cases} \tag{12}$$

From Eqs. (10)-(12), following are derived:

$$\begin{cases} E_{\theta y} = j\dfrac{\eta Ad}{2\lambda r}\sin\theta\cos\theta\cdot\alpha \\ \quad = -\dfrac{\eta Ad}{\lambda r}\sin\theta\cos\theta\sin(kz)\exp(-jkr) \\ E_{\theta z} = -j\dfrac{\eta Ad}{2\lambda r}\sin^2\theta\cdot\beta \\ \quad = -j\dfrac{\eta Ad}{\lambda r}\sin^2\theta\cos(kz)\exp(-jkr) \end{cases} \tag{13}$$

Procedure 3:

$$\begin{cases} E_{\theta y} = -\dfrac{AdRz\omega\mu\sin\left(\omega z\sqrt{\varepsilon\mu}\right)\cdot C}{2\pi\left(R^2+z^2\right)^{(3/2)}} \\ E_{\theta z} = -j\dfrac{AdR^2\omega\mu\cos\left(\omega z\sqrt{\varepsilon\mu}\right)\cdot C}{2\pi\left(R^2+z^2\right)^{(3/2)}} \\ C = \exp\left(-j\omega\sqrt{\varepsilon\mu(R^2+z^2)}\right) \end{cases} \tag{14}$$

Procedure 4:

$$\begin{cases} E_y = -\dfrac{AR\omega\mu}{2\pi}\displaystyle\int_0^{z_{max}}\dfrac{z\sin\left(\omega z\sqrt{\varepsilon\mu}\right)\cdot C}{\left(R^2+z^2\right)^{(3/2)}}dz \\ E_z = -j\dfrac{AR^2\omega\mu}{2\pi}\displaystyle\int_0^{z_{max}}\dfrac{\cos\left(\omega z\sqrt{\varepsilon\mu}\right)\cdot C}{\left(R^2+z^2\right)^{(3/2)}}dz \end{cases} \tag{15}$$

These values E_y, E_z are calculated numerically with actual figures. In the following, the real and imaginary part of calculated value E_y are denoted as E_{yr} and E_{yi}, respectively. Similarly, these parts of E_z are denoted as E_{zr} and E_{zi}.

Procedure 5:

$$\begin{cases} E_y^A = \Re\left[E_y\exp(j\omega t)\right] \\ \quad = E_{yr}\cos(\omega t) - E_{yi}\sin(\omega t) \\ E_z^A = \Re\left[E_z\exp(j\omega t)\right] \\ \quad = E_{zr}\cos(\omega t) - E_{zi}\sin(\omega t) \end{cases} \tag{16}$$

$$\begin{aligned} E &= \sqrt{(E_y^A)^2 + (E_z^A)^2} \\ &= \sqrt{a\cos(2\omega t) - b\sin(2\omega t) + c} \\ &= \sqrt{\sqrt{a^2+b^2}\sin(2\omega t+\theta) + c} \end{aligned} \tag{17}$$

The value θ in the last line above can be fixed by a and b. The values a, b, c in the above equations are as follows:

$$\begin{cases} a = \left(E_{yr}^2 + E_{zr}^2 - E_{yi}^2 - E_{zi}^2\right)/2 \\ b = E_{yr}E_{yi} + E_{zr}E_{zi} \\ c = \left(E_{yr}^2 + E_{zr}^2 + E_{yi}^2 + E_{zi}^2\right)/2 \end{cases} \tag{18}$$

where, every variable such as E_{yr} is fixed numerically by Eq. (16).

According to Eq. (18), the maximum value of E is given at $\sin(2\omega t + \theta) = 1$ and the maximum equals:

$$E_{max} = \sqrt{\sqrt{a^2+b^2}+c}. \tag{19}$$